energies

MDPI

Article

Optimal Design of Horizontal-Axis Tidal Turbine Rotor Based on the Orthogonal Test Method

Xiaojun Zhang [1], Yan Liu [2], Cui Wang [2], Wankun Wang [2] and Honggang Fan [1,*]

[1] Department of Energy and Power Engineering, Tsinghua University, Beijing 100084, China; sdkdzxj@163.com
[2] China Datang Technology Innovation Co., Ltd., Baoding 071700, China; sdailiuyan@163.com (Y.L.); w1456729781@163.com (C.W.); 17854236780@163.com (W.W.)
* Correspondence: fanhg@tsinghua.edu.cn

Abstract

The horizontal-axis tidal turbine is a representative device for harnessing ocean tidal energy, and the structural optimization of its blades is crucial for enhancing the power capture efficiency. In this work, the twist and chord distributions of the blade are determined using an improved Blade Element Momentum (BEM) approach, in which tip and hub loss factors are employed to enhance the modeling accuracy, and these results are employed to construct a parametric model of the original rotor. Due to its simplified assumptions and inability to capture three-dimensional flow effects, computational fluid dynamics (CFD) simulations were carried out to evaluate the hydrodynamic performance and flow analysis of the designed rotor. Further, the orthogonal test method was used to optimize the hydraulic performance of the rotor. Three optimization parameters, namely hub diameter, airfoil type, and maximum airfoil thickness, were set with three levels. Based on the orthogonal design scheme, nine rotor configurations were generated, and their energy capture characteristics and flow fields were subsequently evaluated through numerical simulations. The analysis indicates that the choice of airfoil exerts the strongest impact on the rotor's energy capture efficiency, while the influences of maximum airfoil thickness and hub diameter follow in descending order. Consequently, the optimized rotor adopts a NACA63-415 airfoil with a reduced maximum thickness of 0.9 T_0 and an intermediate hub diameter of 15%R, achieving a power coefficient of 0.445 at the design tip-speed ratio of 4, corresponding to a 3.08% improvement compared with the original design. Flow field analysis demonstrates that the optimized geometry promotes a more uniform spanwise pressure distribution and effectively suppresses flow separation, thereby enhancing the overall hydrodynamic efficiency.

Keywords: horizontal-axis tidal turbine; BEM theory; blade optimization design; hydrodynamic analysis

Academic Editor: Francesco Castellani

Received: 17 November 2025
Revised: 6 January 2026
Accepted: 21 January 2026
Published: 24 January 2026

1. Introduction

As global climate change continues to pose a severe threat to human society, an increasing number of countries have elevated "carbon neutrality" to a national strategic priority. Against this backdrop, the development of clean and renewable energy sources, together with the optimization of energy structures, represents a crucial approach and an effective pathway toward achieving the dual-carbon targets. Ocean energy represents a renewable and environmentally friendly resource with vast potential reserves. The development and utilization of ocean energy have the least impact on the ecological

environment and are conducive to optimizing the energy structure and solving problems such as the energy crisis. Among various forms of ocean energy, tidal power has drawn considerable global interest because of its inherent periodicity, high predictability, and substantial energy density. The horizontal-axis tidal current turbine (HATCT) is among the most commonly employed devices for harnessing tidal power, in which the rotating components convert the kinetic energy of tidal flows into mechanical output. Then the energy is transmitted to the generator end through the transmission mechanism to drive the generator to rotate and convert it into electrical energy. In the energy conversion process, the performance of the conversion is crucial to overall efficiency, while rotor blades are the core components of tidal current power generation devices [1]. Through optimizing the design of the rotor blades, the energy conversion efficiency of tidal current turbines can be greatly improved.

Conventionally, the blade design of a horizontal-axis tidal turbine is carried out through theoretical modeling and optimization-based design strategies. The design of tidal current energy turbine blades is mainly based on BEM theory, which was developed and improved by scholars such as Galuert and Wilson. Bahaj et al. [2] of the University of Southampton in the United Kingdom designed a rotor of a tidal current energy water turbine with a diameter of 0.8 m based on the blade element momentum theory and studied the power characteristics and thrust characteristics of the rotor. Jai N. Goundar [3] designed a 150 kW tidal current energy turbine based on the blade element momentum theory. Its designed rotor has good energy capture efficiency under the condition of an inflow velocity of 1–3 m/s. Sheng Qihu et al. [4] gave the application of the Wilson model to the design of horizontal-axis tidal current energy turbines based on BEM theory, which improved the energy harvesting efficiency of tidal current energy turbines. Chen et al. [5] proposed a calculation to determine the design flow velocity of horizontal-axis tidal current turbine blades to improve energy capture efficiency under variable sea current conditions. By combining the BEM theory with Wilson's optimization method, the study achieved good agreement between experimental and numerical results, validating the effectiveness of the proposed approach.

Advances in computational technology have made multi-parameter optimization increasingly feasible, enabling its widespread application in the design of turbine rotor blades. Li Zhenqi et al. [6] combined the artificial neural network (ANN) with the genetic algorithm (GA) to optimize the blade geometry of a tidal current turbine. The ANN served as a surrogate model for GA optimization, accelerating the iterative process and achieving up to an 8.5% improvement in energy conversion efficiency compared with the original rotor. Li Changming et al. [7] proposed a coupled deep learning and blade element momentum (DL-BEM) optimization framework, which effectively predicted hydrodynamic performance with reduced computational cost and obtained a better balance between power coefficient and thrust coefficient. Wang Yongding et al. [8] optimized the NACA4412 airfoil for tidal turbine blades using the Joukowski conformal transformation and a Genetic Algorithm (GA) with the maximum lift–drag ratio as the objective function. CFD simulations showed that the optimized hydrofoil achieved increases of 18.72% in maximum lift coefficient and 46.84% in maximum lift–drag ratio compared with the original profile. Such optimization studies typically require establishing a response relationship between design parameters and turbine performance, which involves evaluating a large number of turbine configurations and consequently demands substantial computational resources.

The orthogonal optimization approach offers an efficient means of evaluating the influence of multiple design parameters while requiring significantly fewer computational resources. It is currently widely used in the optimization of rotating machinery impeller blades. Using an orthogonal design strategy enables researchers to efficiently identify

representative test configurations and carry out the optimization process with significantly reduced effort. Li Yanpin et al. [9] constructed a four-factor and three-level orthogonal table. The research found that the number of blades has the greatest impact on the performance of the hydraulic turbine rotor. By selecting appropriate parameters, the efficiency of the optimized hydraulic turbine rotor was improved by 1.74%. Wang Chenyang [10] designed an orthogonal test with four factors and three levels and used CFX software to analyze the impact of different factors on the performance of the water turbine. The efficiency of the optimized water turbine under rated operating conditions was 2.04% higher than that of the original water turbine, and the internal flow field distribution was better. Numerous studies [11–14] have successfully applied the orthogonal optimization approach to develop rotor designs with superior hydrodynamic performance, thereby demonstrating the effectiveness of this method.

The hydrodynamic performance of horizontal-axis tidal turbines with various structural parameters has been extensively studied through theoretical modeling and numerical simulations in the literature review above. On this basis, different optimization methods have been applied to rotor design, yet many rely on computationally intensive iterative processes or data-driven AI frameworks that require substantial numerical resources. Furthermore, some research focuses on single parameter modifications, while the synergistic effects of multiple geometric factors on energy capture efficiency remain relatively underexplored.

In this work, a practical and computationally economical optimization strategy for a horizontal-axis tidal current turbine is proposed by combining blade element momentum theory, computational fluid dynamics, and the orthogonal test method. An improved BEM theory is employed to establish a baseline blade geometry, while CFD simulations are used to evaluate rotor performance and flow characteristics. To improve the energy capture efficiency of a horizontal-axis tidal current turbine rotor, three factors are selected as follows: hub diameter, airfoil type, and maximum airfoil thickness, and a three-factor and three-level orthogonal table is established. Finally, the hydrodynamic performance of the optimized rotor is analyzed and compared with the original rotor to prove the effectiveness of the orthogonal optimization method. Compared with recent studies that rely on exhaustive CFD iterations or purely theoretical models, the proposed approach offers a balance between computational economy and physical accuracy, thereby providing practical design guidance for preliminary tidal turbine rotor development.

2. Design Theory and Method of Tidal Current Energy Turbine Rotor

2.1. Rotor Design Theory

Because the structural configuration of a horizontal-axis tidal turbine closely resembles that of a horizontal-axis wind turbine, its blade design approach similarly draws inspiration from wind turbine aerodynamics. Among the available analytical methods, the blade element momentum (BEM) theory remains the most extensively adopted tool for estimating rotor loading and overall performance. Originally developed by Glauert, BEM integrates classical blade element theory with momentum analysis to assess the aerodynamic behavior of aircraft propellers. The blade element theory divides the blade span into numerous small segments of width dr, each treated as an independent two-dimensional airfoil. The aerodynamic forces generated by all such blade elements are then integrated to determine the overall thrust and torque acting on the rotor. The corresponding velocity triangle and force analysis for a representative blade element are illustrated in Figure 1.

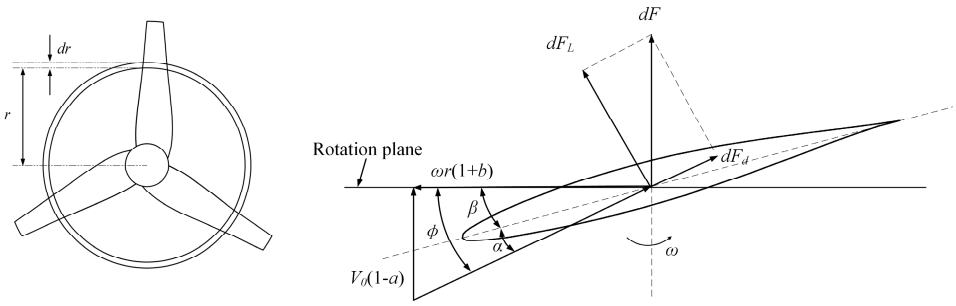

Figure 1. Forces on a single blade element.

According to the momentum theory, the relative inflow velocity W of the blade element dr is as follows:

$$W = \sqrt{V_0{}^2(1-a)^2 + (\omega r)^2(1+b)^2} \tag{1}$$

$$\varphi = \alpha + \beta = \arctan\frac{(1-a)V_0}{(1+b)\omega r} \tag{2}$$

where W is the relative incoming velocity; V_0 is the incoming velocity; φ is the inlet angle; ω is the rotational angular velocity; α is the angle of attack; and β is the pitch angle; a and b are the axial and tangential induction factors.

The lift and drag forces acting on the impeller leaf vein dr are as follows:

$$dF_L = \frac{1}{2}\rho W^2 c C_L dr \tag{3}$$

$$dF_D = \frac{1}{2}\rho W^2 c C_D dr \tag{4}$$

where c is the impeller chord length; C_L is the lift coefficient; C_D is the drag coefficient; and r is the position of the impeller radius where this impeller is located.

By projecting the lift F_L and drag F_D to the axial and tangential directions of the impeller, the axial force F_a and tangential force F_t of the impeller can be obtained with the following expressions:

$$dF_a = dF_L\cos\varphi + dF_D\sin\varphi = \frac{1}{2}\rho W^2 c(C_L\cos\varphi + C_D\sin\varphi)dr \tag{5}$$

$$dF_t = dF_L\sin\varphi - dF_D\cos\varphi = \frac{1}{2}\rho W^2 c(C_L\sin\varphi - C_D\cos\varphi)dr \tag{6}$$

The thrust coefficient and torque coefficient can be defined as follows:

$$C_T = C_L\cos\varphi + C_D\sin\varphi \tag{7}$$

$$C_M = C_L\sin\varphi - C_D\cos\varphi \tag{8}$$

If the impeller has B blades, the thrust d_T and torque d_M acting on the impeller blade vane dr are as follows:

$$dT = \frac{1}{2}B\rho c W^2 C_T dr \tag{9}$$

$$dM = \frac{1}{2}B\rho c W^2 C_M dr \tag{10}$$

The chord length real degree δ is expressed as the ratio of the total blade chord length to the perimeter of the radius where it is located for a given radius as follows:

$$\delta = \frac{Bc}{2\pi r} \tag{11}$$

The axial induction factor a and the circumferential induction factor b can be obtained by iteratively solving the following equations:

$$\frac{a}{1-a} = \frac{\delta C_T}{4\sin^2\varphi} \tag{12}$$

$$\frac{b}{1+b} = \frac{\delta C_M}{4\sin\varphi\cos\varphi} \tag{13}$$

Utilizing a custom BEM algorithm implemented in MATLAB R2024b, the axial and circumferential induction factors are computed through an iterative process based on momentum theory. Subsequently, the specific chord length and pitch angle distributions are derived for every blade element.

The tip-speed ratio is the ratio of the turbine tip speed to the incoming flow speed:

$$TSR = \frac{\omega r}{V_0} \tag{14}$$

The turbine power coefficient C_p, thrust coefficient C_T are given by the following:

$$C_p = \frac{M\cdot\omega}{0.5\rho A {V_0}^3} \tag{15}$$

$$C_T = \frac{T}{0.5\rho A {V_0}^2} \tag{16}$$

where M is the output torque of the turbine shaft end; T is the thrust of the turbine; ω is the rotational angular velocity of the turbine; ρ is the fluid density; A is the swept area of the turbine blades; and V_0 is the incoming flow velocity.

2.2. Rotor Design Parameters and Process

The first step in designing tidal current turbines is to select the appropriate blade airfoil. Referring to existing research, it is found that the NACA63-4XX series airfoils have high lift–drag ratios within a certain range of attack angles and have a strong ability to withstand loads, so they are widely used in the design of horizontal-axis tidal current turbine rotor blades [15]. The NACA63-412 airfoil is selected for the blade section airfoil in this paper. The geometric shape of this airfoil is shown in Figure 2.

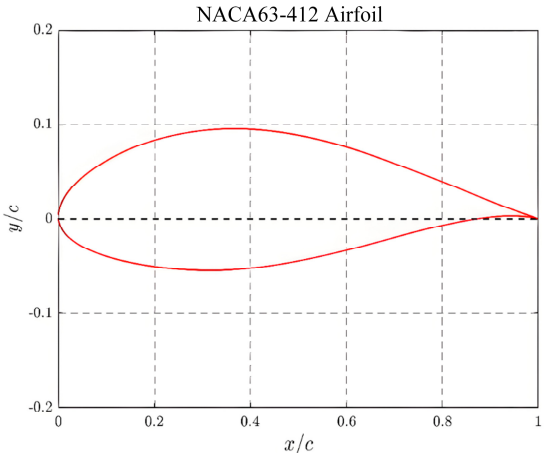

Figure 2. NACA63-412 airfoil geometry.

In general, the tidal current energy utilization coefficient is positively correlated with the number of blades. When the number of blades is greater than 3, the rate at which the tidal current energy utilization coefficient increases with the number of blades decreases and is accompanied by an increase in design and production costs. Therefore, considering all factors, the number of blades is set to 3. For a tidal current turbine rotor with three blades, the typical tip-speed ratio is either 3 or 4. To enhance the overall energy capture efficiency, the blade tip-speed ratio in this study is set to 4. The experimental platform can provide an incoming flow velocity of 2 m/s, the impeller blade diameter is 0.25 m, and the design power coefficient is 0.35. The overall design parameters are shown in Table 1.

Table 1. Basic design parameters.

Parameters (Units)	Data
design power factor	0.35
rotor diameter (m)	0.25
hub diameter (m)	0.05
Blade number	3
rotational speed (r/min)	611.15
inlet velocity (m/s)	2
fluid density (kg/m^3)	998.2
design tip-speed ratio	4

According to the blade element–momentum theory, the blade span is discretized into 11 sections with a 7 mm interval. Including the hub region, the blade consists of 12 sections in total. Each section is defined by its own chord length and pitch angle.

According to the Wilson theory, the power coefficient calculation formula is deduced to obtain the objective function to be optimized as follows:

$$\frac{dC_p}{d\lambda} = \frac{8b(1-a)F\lambda^3}{{\lambda_0}^2} \tag{17}$$

where: a is the axial induction factor; b is the circumferential induction factor; F is the Prandtl correction factor; λ_0 is the design blade tip-speed ratio; and λ is the tip-speed ratio of different blade element sections.

To obtain maximum energy harvesting efficiency, $dC_p/d\lambda$ on each leaf element cross-section must be maximized. Equation (16) is used as the objective function, and constraint Equation (17) and solution Equation (18) are, respectively, as follows:

$$\begin{cases} a(1-aF) = b(1+b)\lambda^2 \\ F = F_{tip} \cdot F_{hub} \\ F_{tip} = \frac{2}{\pi} ar\cos(\exp(-\frac{B(R-r)}{2R\sin\varphi})) \\ F_{hub} = \frac{2}{\pi} ar\cos(\exp(-\frac{B(r-r_{hub})}{2r_{hub}\sin\varphi})) \\ \tan\varphi = \frac{V_0(1-a)}{\omega r(1+b)} = \frac{(1-a)}{(1+b)}\frac{1}{\lambda} \end{cases} \tag{18}$$

$$\begin{cases} \frac{BcC_L}{r} = \frac{8\pi aF(1-aF)}{(1-a)^2}\frac{\sin^2\varphi}{\cos\varphi} \\ \beta = \varphi - \alpha \end{cases} \tag{19}$$

where F_{tip} is the tip loss factor, and F_{hub} is the hub loss factor.

To facilitate the theoretical calculation of rotor design parameters and to visualize their variations more intuitively, a MATLAB-based graphical user interface (GUI) was developed. The program, built upon the BEM theory, enables the design and analysis of

horizontal-axis tidal current turbine rotors within a single integrated platform. Figure 3 shows the flowchart of the algorithm used in the program.

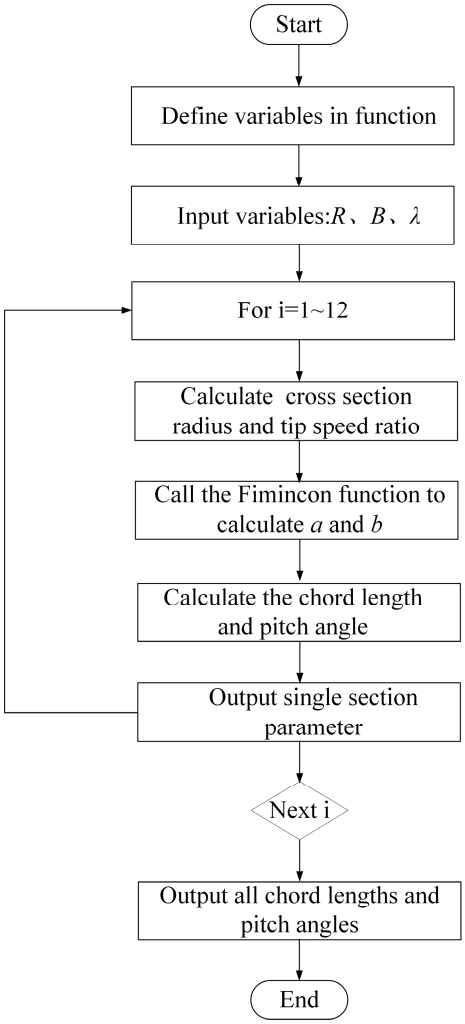

Figure 3. Flowchart of the algorithm used in the program.

Table 2 presents the calculated blade-geometry parameters for a 0.25 m diameter rotor operating at an optimal *TSR* of 4. To further illustrate the design, Figure 4 shows the distributions of the blade geometric parameters, and Figure 5 provides the corresponding 3D blade model.

Table 2. Design parameters of each blade section.

r/R	r (mm)	c (mm)	β (deg)
0.384	48	37.07	17.41
0.44	55	34.22	15.17
0.496	62	31.60	13.32
0.552	69	29.25	11.76
0.608	76	27.14	10.42
0.664	83	25.26	9.27
0.72	90	23.57	8.24
0.776	97	22.02	7.33
0.832	104	20.55	6.48
0.888	111	19.07	5.67
0.944	118	17.31	4.84
1	125	14.16	3.91

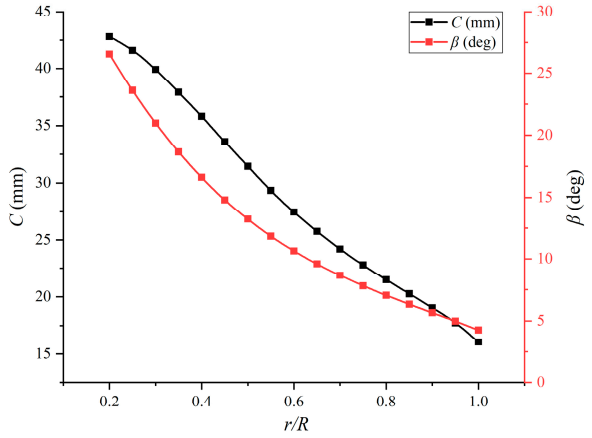

Figure 4. Distributions of chord length and twist angle of the original blade.

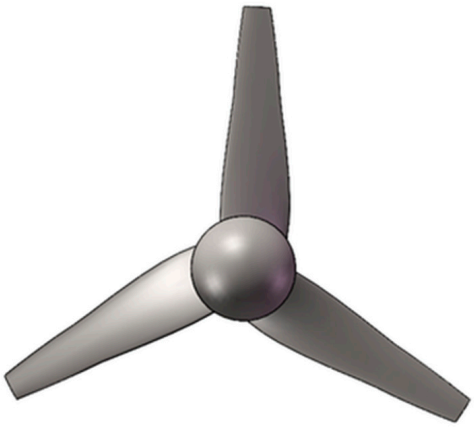

Figure 5. Original blade 3D model.

3. Numerical Simulation

3.1. Computing Domain and Grid Division

Owing to the low-order nature of blade element momentum (BEM) theory and its limited accuracy in capturing complex three-dimensional flow effects, computational fluid dynamics (CFD) simulations are employed in this study to more accurately evaluate the hydrodynamic performance of the tidal turbine rotor. To model the rotational behavior of the horizontal-axis tidal turbine rotor, the computational domain is constructed as a cylindrical region, as illustrated in Figure 5. For ease of mesh generation and to correctly represent rotor motion, the domain is partitioned into an inner rotating region and an outer stationary region. Because the flow within the rotor's rotating region is highly complex and detailed observation of blade-surface flow behavior is required, a higher mesh resolution is necessary in this zone. Consequently, both the grid density and accuracy in the rotating domain are enhanced to ensure reliable capture of local flow features. Since the flow in the stationary domain is relatively uniform and exhibits minimal variation, high mesh resolution is not required in this region. To reduce computational cost and shorten simulation time, the grid density in the static domain is, therefore, appropriately coarsened. In order to unify the reference value, the size of the calculation domain in this paper uses the rotor diameter D as the reference value. To ensure sufficient flow development and avoid non-uniform inlet conditions, the computational domain is extended to a length equal to 15 times the rotor diameter, while the upstream inlet diameter is set to five times the rotor diameter.

Based on the original model and the above-mentioned fluid region modeling, fluent meshing is imported for grid division, and the overall computing domain of the hydraulic turbine is grid-division using a poly-hex core unstructured grid. To accurately account for the boundary layer effects on the numerical results, the mesh density is increased near the walls and blade surfaces. Furthermore, local grid refinement is applied to regions exhibiting significant flow fluctuations. Figure 6 shows the specific grid details.

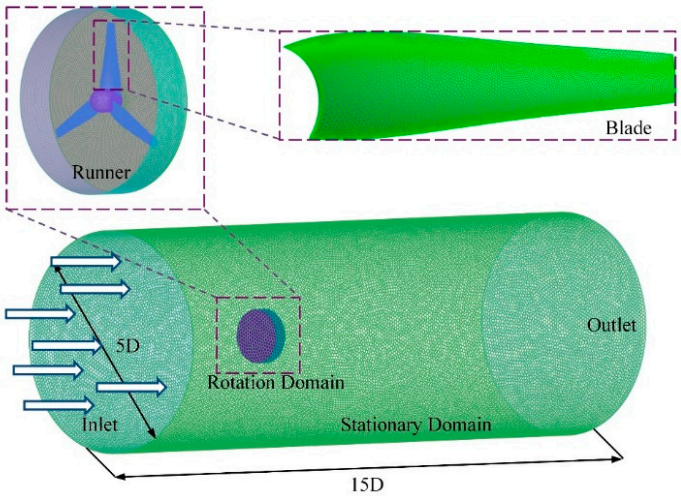

(**a**) Computational domain and grid

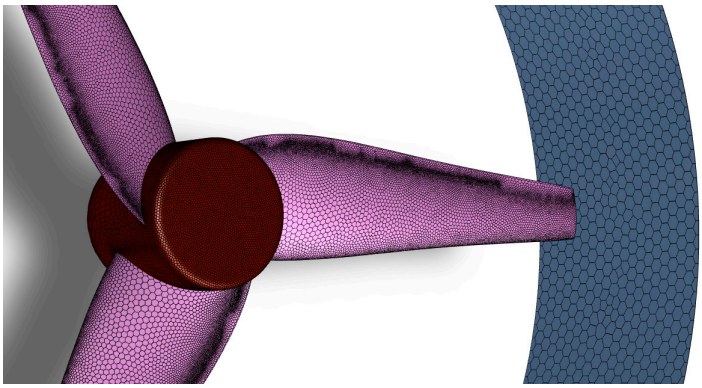

(**b**) Blade surface mesh details

Figure 6. Computational domain and grid model detail.

To accurately capture the viscous effects within the boundary layer, the mesh resolution near the blade surfaces was carefully controlled. As shown in Figure 7, the y+ values on the majority of the blade surface are less than 1, and a minority region near the blade tip exhibits slightly higher y+ values due to elevated local flow velocities. Considering the adoption of the SST *k-w* model for the calculations, the distribution of y+ values conformed to the computational requirements.

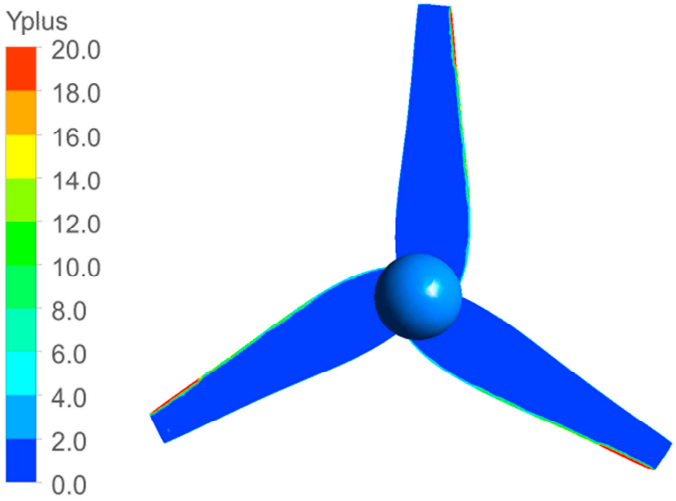

Figure 7. Y^+ distribution of the blade.

3.2. Grid Independence Verification

The grid resolution directly affects the accuracy of the numerical results: an insufficient number of cells may compromise precision, whereas an excessively refined mesh leads to unnecessary computational cost. Consequently, a grid independence study must be performed prior to the main simulations.

To assess mesh independence, three grid configurations with varying numbers of elements were evaluated. The power coefficient of the tidal turbine rotor at the design operating condition (TSR = 4) was computed for each case, and the results are listed in Table 3. As the mesh density increased, the predicted power coefficient gradually converged, and the relative error decreased accordingly. Once the total number of mesh elements exceeded 2,870,570, the relative error of the power coefficient fell below 0.043. Balancing computational cost with solution accuracy, the second mesh configuration containing 2,870,570 elements was selected for all subsequent simulations.

Table 3. Grid convergence results.

Grid	Static Domain	Rotation Domain	Total	Power Coefficient	Relative Error
$Grid_1$	280,587	734,685	1,015,272	0.414	0
$Grid_2$	1,473,239	1,397,331	2,870,570	0.432	0.043
$Grid_3$	2,303,015	2,168,622	4,471,637	0.433	0.046

3.3. Boundary Condition Settings

The moving reference frame (MRF) approach is extensively employed for predicting the hydrodynamic behavior of tidal turbines, owing to its high computational efficiency and reliability [16,17]. Therefore, the MRF approach is coupled with the SST k-ω turbulence model to compute the rotor torque (Q) and thrust (T), from which the power coefficient C_P and thrust coefficient C_T are subsequently obtained. The inlet boundary is set as a uniform velocity condition, while the outlet is defined using a static pressure boundary. Within the rotating region, the blade and hub surfaces are treated as no-slip walls, and the outer cylindrical surface of the computational domain is likewise specified as a no-slip boundary. The stationary and rotating domains are coupled through a designated interface to ensure proper exchange of flow information.

In airfoil hydrodynamic simulations, the SST K-ω turbulence model has demonstrated strong consistency with experimental observations, indicating its suitability for accurately capturing flow features. In addition, the SST K-ω model is more accurate in calculating the near-wall area, wake, and flow around the airflow. Therefore, the SST K-ω model is

selected as the calculation model [18,19]. The solution is based on the SIMPLE algorithm of velocity and pressure coupling. The discretization adopts the standard form.

To maintain a high level of numerical accuracy, a second-order upwind discretization scheme is employed in the simulations.

3.4. Numerical Simulation Results

The computational mesh described above is employed to evaluate the hydrodynamic characteristics of the designed tidal turbine rotor. In the simulations, an inflow velocity of 2.0 m/s is prescribed, while the rotor's rotational speed is adjusted to represent various tip-speed ratio conditions. This setup enables the determination of the relationship between the rotor power coefficient C_p and the tip-speed ratio λ. Figure 8 indicates that, within the tip-speed ratio interval of 3.5 to 6, the rotor's power coefficient initially rises and subsequently declines as the *TSR* continues to increase. When *TSR* = 4.5, the power coefficient reaches a maximum value of 0.432, achieving the design target. Moreover, the overall operation of the turbine is stable, the tip-speed ratio is within the range of [3.5–5.5], the turbine power coefficient is maintained above 0.395, the operating range is wide, and it meets the design requirements.

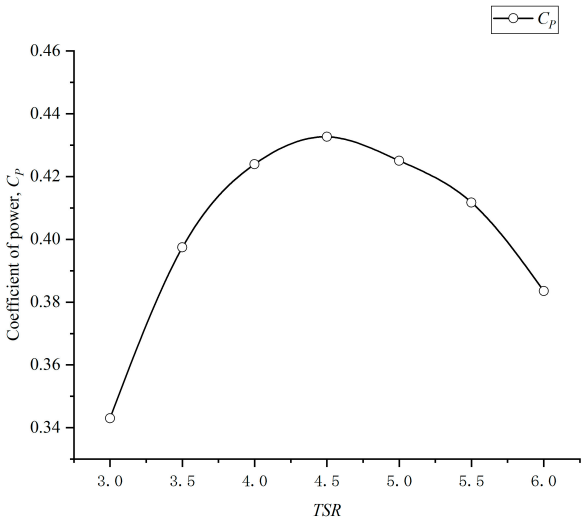

Figure 8. Curve of the original rotor power coefficient changing with tip-speed ratio.

4. Rotor Optimization Design

4.1. Orthogonal Optimization Scheme Design

The orthogonal design approach is an effective technique for organizing and analyzing optimization problems involving multiple parameters, substantially enhancing the overall efficiency of the optimization process. This method is characterized by the following three fundamental components: the orthogonal parameter, parameter level, and orthogonal table. To improve the performance of tidal energy turbines, the power coefficient and the thrust coefficient are taken as the optimization targets. The following three factors are selected: hub diameter (factor A), airfoil type (factor B), and maximum airfoil thickness (factor C). Three levels are selected for each factor. A three-factor, three-level orthogonal table is constructed to perform orthogonal optimization design. The optimization factor levels are shown in Table 4.

A1 indicates the hub diameter is 10%*R*, A2 indicates the hub diameter is 15%*R*, and A3 indicates the hub diameter is 20%*R*; B1 indicates the airfoil type is NACA63-412, B2 indicates the airfoil type is NACA63-415, and B3 indicates the airfoil type is S-809; C1 means the maximum thickness of the airfoil is $0.9T_0$, C2 means the maximum thickness of the airfoil is T_0, and C3 means the maximum thickness of the airfoil is 1.1 T_0. According

to the orthogonal principle, the $L_9(3^3)$ orthogonal table is selected, and the experimental scheme is shown in Table 5.

Table 4. Orthogonal optimization factor level table.

Level	Factor		
	Hub Diameter	**Airfoil Type**	**Maximum Airfoil Thickness**
1	A1	B1	C1
2	A2	B2	C2
3	A3	B3	C3

Table 5. Orthogonal table.

Individual No.	Factor		
	Hub Diameter	**Airfoil Type**	**Maximum Airfoil Thickness**
1	A1	B1	C1
2	A1	B2	C2
3	A1	B3	C3
4	A2	B1	C2
5	A2	B2	C3
6	A2	B3	C1
7	A3	B1	C3
8	A3	B2	C1
9	A3	B3	C2

4.2. Orthogonal Test Results and Analysis

Nine tested tidal turbine rotors with different parameter levels were first designed, and then the numerical simulation was conducted to obtain the power coefficient and thrust coefficient. Table 6 shows the simulated tidal turbine power coefficient and thrust coefficient for different individuals at the designed blade tip-speed ratio. The tidal turbine power coefficient is in a range of 0.296 to 0.438.

Table 6. Orthogonal optimization test results.

Individual No.	λ	C_p
1	4	0.434
2	4	0.428
3	4	0.296
4	4	0.421
5	4	0.426
6	4	0.368
7	4	0.420
8	4	0.438
9	4	0.353

To quantify the impact of each specific parameter within the orthogonal experimental design, the mean power coefficient ($\overline{K_i}$) is calculated using the following equation:

$$\overline{K_i} = \frac{1}{N}\sum_{j=1}^{N} P_j \tag{20}$$

where i is the level of parameter; N is the individual number of the corresponding parameter at level I; and P_j is the power coefficient of the tested tidal turbine rotor with level i. The average value of the thrust coefficient is defined by the same formula.

The range (R) serves as a metric to quantify the significance of each parameter's impact. It is calculated using the expression below:

$$R = \max(\overline{K_i}) - \min(\overline{K_i}), i = 1, 2, 3, 4 \tag{21}$$

Table 7 presents the range analysis results regarding the impact of each factor on the power coefficient. According to the results of the range analysis, the influence of each factor level on the optimization target can be obtained. The influence on the power coefficient is ranked as follows: B > C > A. While it has the maximum value at A2, B2, and C1.

Table 7. Power coefficient range analysis.

C_P	Factor		
	A	**B**	**C**
$\overline{K1}$	0.386	0.425	0.413
$\overline{K2}$	0.405	0.431	0.401
$\overline{K3}$	0.404	0.339	0.381
R	0.019	0.092	0.032
Sequence	3	1	2

In orthogonal experiments, analysis of variance (ANOVA) is used to quantitatively assess the influence of each design factor on the response. The total sum of squares is defined as follows:

$$SS_T = \sum_{j=1}^{N} (y_j - \overline{y})^2 \tag{22}$$

where y_j is the power coefficient obtained in the j-th experiment; $\overline{y}$ is the average of all test results; and N represents the total number of tests.

For the i-th design factor, its sum of squares is expressed as follows:

$$SS_i = \sum_{k=1}^{L} n_k (\overline{y}_{ik} - \overline{y}) \tag{23}$$

where L represents the number of levels for this factor; n_k is the number of times the k-th level appears in the orthogonal table; and $\overline{y}_{ik}$ represents the average response value of the factor at the k-th level.

The sum of squared errors is obtained by the following formula:

$$SS_E = SS_T - \sum SS_i \tag{24}$$

The sensitivity of each factor to the power coefficient is measured by the contribution ratio, which is defined as follows:

$$CR_i = \frac{SS_i}{SS_T} \times 100\% \tag{25}$$

The larger the contribution rate, the more significant the impact of this factor on performance changes. As shown in Table 8, the airfoil type (Factor B) dominates the variation of the power coefficient, contributing 83.67% of the total variance, which is consistent with the results obtained from the range analysis. The maximum airfoil thickness (Factor C) and hub diameter (Factor A) play secondary roles, with contribution ratios of 8.60% and 3.57%, respectively. The remaining variation is attributed to numerical uncertainty. This analysis quantitatively confirms that airfoil selection is the primary factor governing the hydrodynamic performance of the tidal turbine rotor.

Table 8. ANOVA and sensitivity analysis for the power coefficient.

Factor	*DOF*	*SS*	CR_i
A	2	0.000675	3.57%
B	2	0.015831	83.67%
C	2	0.001628	8.60%
Error	2	0.000788	4.16%
Total	8	0.018922	100%

4.3. Orthogonal Optimization

Taking the design objectives and optimization analysis into account, the optimal combination of parameter levels is determined to be A2, B2, and C1. The selected parameter levels for both the original and optimized turbine rotors are summarized in Table 9.

Table 9. Levels of three parameters for the original rotor and the optimal rotor.

Rotor	Levels of Three Parameters		
	A	B	C
Original rotor	20%*R*	NACA63-412	T_0
Optimal rotor	15%*R*	NACA63-415	$0.9T_0$

Figure 9 presents a comparison of the geometric characteristics of the original rotor and the optimal rotor.

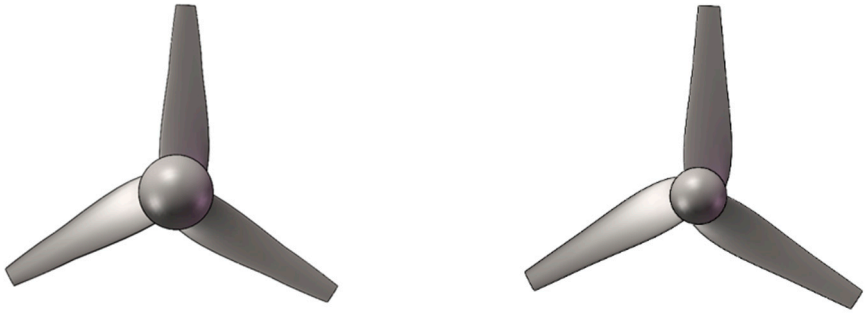

(**a**) Original rotor geometry (**b**) Optimal rotor geometry

Figure 9. Comparison between the original rotor and optimal rotor.

4.4. Optimized Tidal Turbine Rotor Performance Analysis

4.4.1. Hydrodynamic Performance

Figure 10 presents the variations in power coefficient (a) and thrust coefficient (b) for both the original and optimized rotors over a tip-speed ratio range of 3.5 to 6. The power-coefficient profiles of the two rotor configurations exhibit a characteristic parabolic trend within this interval. The observed parabolic trend of C_P with respect to *TSR* is consistent with BEM theory. At low *TSR*, the axial induction factor is small, and the high angle of attack may lead to a stall on the blade sections. Conversely, at high TSR, the increased rotational speed leads to higher tip losses and increased drag torque, thus reducing the power extraction. From the curve of the power coefficient changing with the tip-speed ratio, within the range of the tip-speed ratio, the power coefficient of the optimized rotor is always higher than that of the original rotor, and when *TSR* = 4 is the design condition, the power coefficient of the optimized rotor is 3.08% higher than that of the original rotor. The improvement can be attributed to the enhanced pressure difference between the pressure and suction pressure of the blade. This means that the optimized rotor can capture more

tidal energy in the same time and convert it into more electrical energy in actual engineering applications.

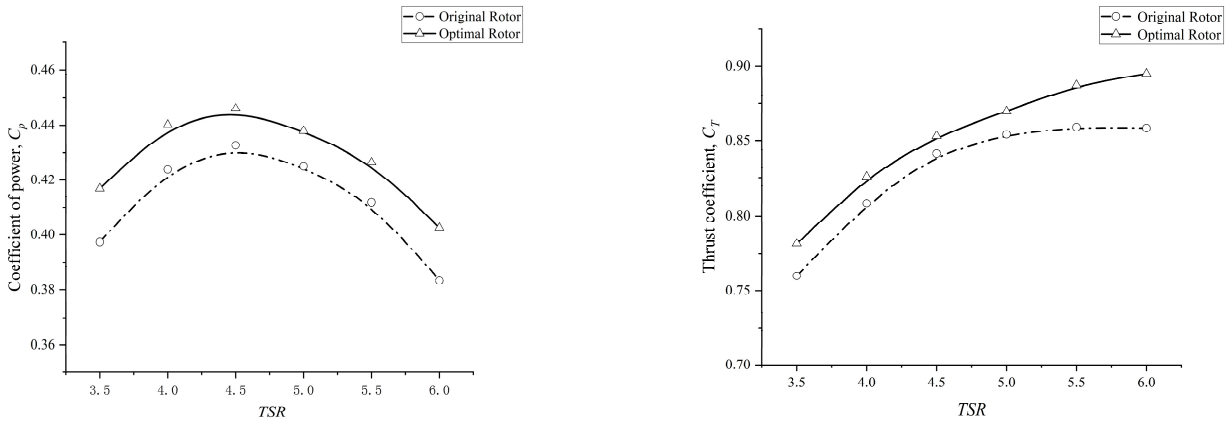

Figure 10. Distribution of turbine power coefficient and thrust coefficient under different tip-speed ratios: (**a**) power coefficient variation curve with tip-speed ratio; (**b**) thrust coefficient changing curve with tip-speed ratio.

An examination of the thrust-coefficient curves before and after optimization indicates that the optimized rotor consistently outperforms the original one across the entire simulated tip-speed ratio range. Moreover, the performance gap between the two designs widens as the tip-speed ratio increases. At the design condition of TSR = 4, the thrust coefficient of the optimized rotor is elevated by approximately 2.22% compared with the original rotor, implying a larger axial force acting on the optimized rotor. This increased axial loading enhances the torque output of the tidal turbine and contributes to improved self-starting capability.

To further contextualize the performance of the optimized rotor, a comparative analysis was performed against representative horizontal-axis tidal turbine designs from recent literature, as summarized in Table 10. The results in Table 10 indicate that the optimized rotor developed in this study possesses a highly competitive energy capture capability. However, a significant advantage of the present design is its structural load characteristic. The thrust coefficient (CT) of 0.826 is notably lower than that of other designs with similar efficiency, which typically range from 0.859 to 0.962. A lower C_T implies reduced axial loading on the blade structure and mooring system, which is critical for mitigating fatigue and enhancing the operational stability of tidal energy turbines.

Table 10. Comparison of hydrodynamic performance between the optimized rotor and representative designs.

Rotor Source	Optimal *TSR*	C_p	C_T
Present work	4.5	0.445	0.826
Alipour R et al. [20]	5.0	0.358	0.962
Xu B et al. [21]	6.0	0.446	0.859
Li et al. [7]	5.0	0.452	0.916
Wang et al. [22]	4.6	0.402	-

4.4.2. Pressure Distribution

Figure 11 presents the pressure contours at various spanwise locations for both the baseline and optimized rotors at TSR = 4, offering a detailed view of their hydrodynamic behavior. At any given radial section, peak positive and negative pressures are concentrated

near the leading edge. As the radial position increases, the pressure differential between the pressure and suction surfaces widens significantly. This phenomenon is attributed to the rise in local circumferential velocity with radius, which amplifies the local dynamic pressure and strengthens the lift-generating pressure difference. In accordance with Blade Element Momentum (BEM) theory, this augmented pressure differential contributes directly to higher torque generation, constituting the primary driving force for the rotor.

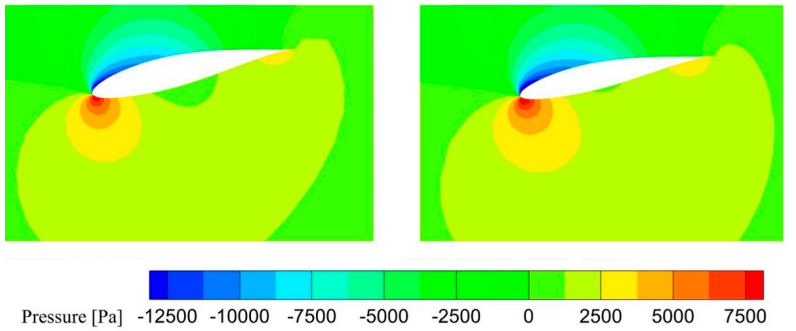

(**a**) $r/R = 0.5$

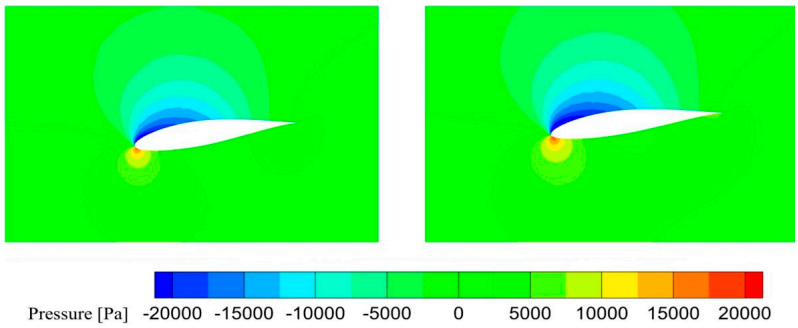

(**b**) $r/R = 0.7$

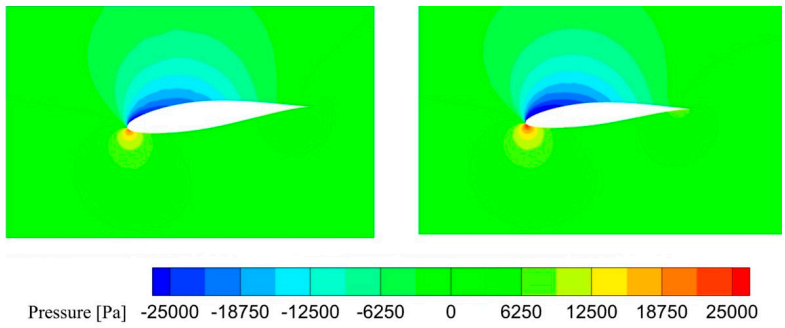

(**c**) $r/R = 0.9$

Figure 11. The pressure contour maps of blade cross sections at different r/R positions (**left**: original rotor; **right**: optimized rotor).

Following the optimization, the adjusted geometric parameters of the rotor enable the incoming flow to distribute more uniformly across the blade surface, which diminishes the likelihood of flow separation and enhances the rotor's overall hydrodynamic performance. Although the minimum pressure on the suction-side low-pressure region remains comparable between the two designs, the optimized hydrofoil exhibits a noticeably larger low-pressure area. In general, an expanded high-pressure region on the pressure side together with an enlarged low-pressure region on the suction side contributes to stronger pressure differentials, thereby improving the energy capture capability of the horizontal-axis tidal turbine rotor. Furthermore, the broadened high-pressure distribution

helps homogenize the blade loading, significantly improving the operational stability of the tidal turbine.

For a more rigorous quantification of the hydrodynamic loading, the chordwise pressure difference (ΔP) profiles are investigated across representative sections. As shown in Figure 12, the optimized rotor demonstrates a systematic augmentation of the pressure differential along the majority of the chord, with the most pronounced enhancement concentrated in the leading-edge region. This indicates that the refined blade geometry facilitates a more effective and favorable chordwise pressure distribution, which underpins the physical mechanism for the observed 3.08% improvement in the power coefficient.

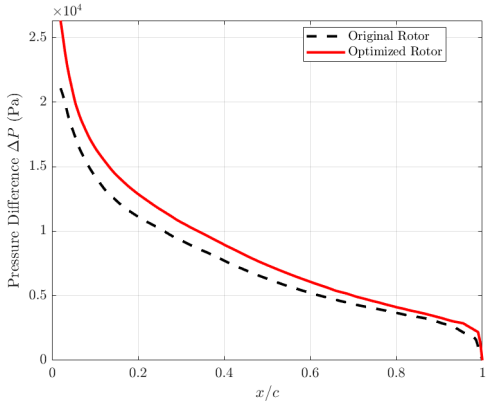

(**a**) $r/R = 0.5$

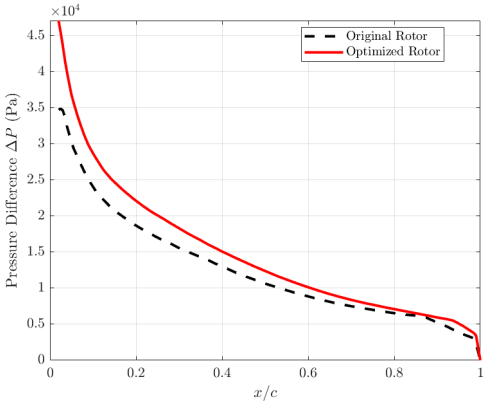

(**b**) $r/R = 0.7$

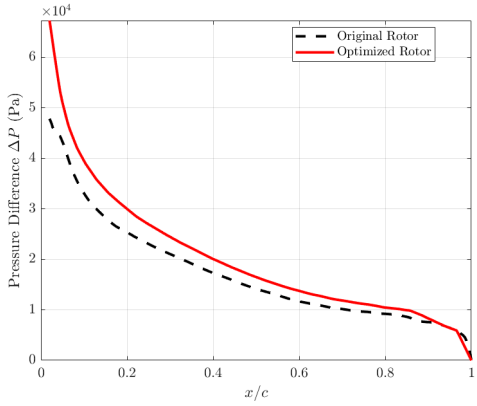

(**c**) $r/R = 0.9$

Figure 12. The pressure difference (ΔP) maps of blade cross sections at different r/R positions.

4.4.3. Pressure Coefficient Distribution

Figure 13 shows the comparison of pressure coefficient distributions along different sections of the rotor blade at the design tip-speed ratio, $TSR = 4$. The horizontal axis is normalized, where c is the chord length on different sections. Under the current working conditions, the pressure distribution on the airfoil's upstream surface is larger, which appears as a pressure surface; the pressure distribution on the airfoil's downstream surface is relatively smaller, which appears as a suction surface. Across various radial sections, the optimized blade exhibits a higher pressure coefficient on the pressure side compared to the baseline design. Conversely, the pressure distribution on the suction surface remains largely consistent between the two rotors. Consequently, the optimized rotor demonstrates a more significant pressure differential across the hydrofoil sections, leading to enhanced lift generation relative to the baseline model. This improvement directly translates into higher rotational torque. Ultimately, the observed increase in energy extraction capability substantiates the efficacy of the orthogonal design method for optimizing rotor performance.

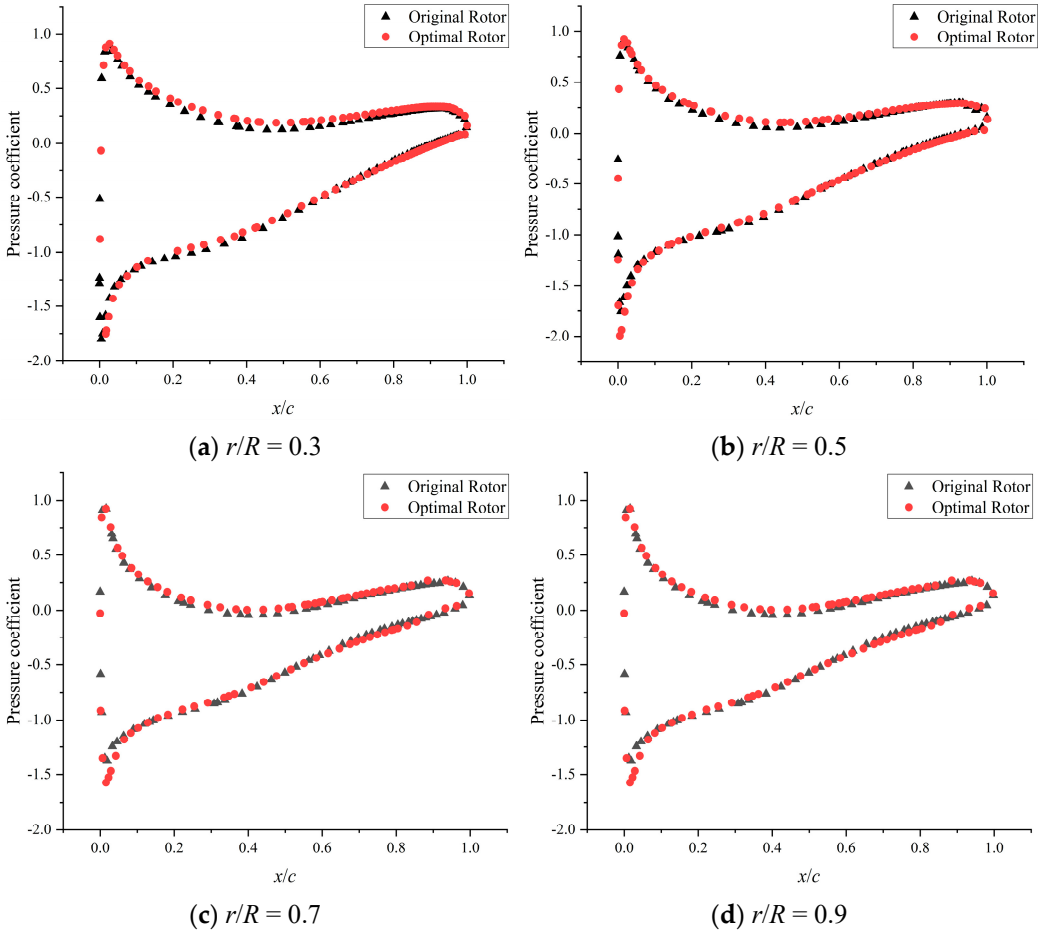

Figure 13. The distribution of the pressure coefficient curve of the rotor blades at TSR = 4.

Figure 14 compares the integrated lift coefficients (C_l) of the original and optimized rotors across various radial positions. Although both designs follow a characteristic downward trend in C_l from hub to tip, the optimized rotor consistently maintains higher values at every section. These improvements are particularly significant in the mid to outer regions (r/R = 0.5–0.9), where the refined airfoil selection and thickness distribution effectively widen the pressure differential between the blade surfaces. This elevated sectional lift

translates directly into higher torque, thereby underpinning the substantial gains in overall power coefficient.

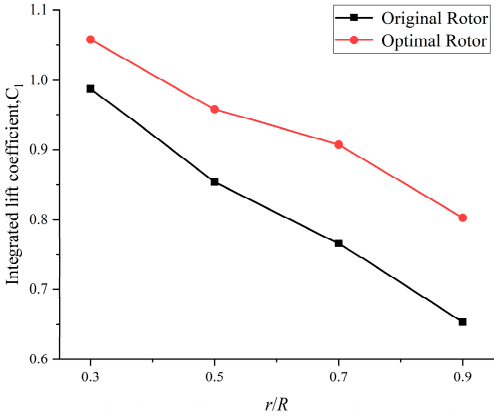

Figure 14. Comparison of integrated sectional lift coefficient (C_l) along the blade span at *TSR* = 4.

4.4.4. Vortex Structure

Figure 15 shows the vortex structures shed from both the original and optimized rotors under tip-speed ratios between 4 and 6. The *Q*-criterion is employed as the vortex detection method, enabling the characterization of localized flow features commonly observed in turbomachinery, including tidal turbines and marine propellers [23–25]. The simulation results indicate that under different tip-speed ratios, the leakage vortex predominantly occurs in the blade tip region, whereas only an attachment vortex is observed near the blade root region. At low tip-speed ratios, pronounced vortex leakage occurs near the hub trailing region, and the optimized rotor exhibits stronger vortex intensity in this area. As the *TSR* increases, the vortex intensity at the hub tail gradually weakens. Due to the rotor's rotation, both the original and optimized rotors generate stable spiral tip vortices, with their vortex trajectories clearly visible. As the tip-speed ratio increases, the vortex intensity is enhanced in both the original and optimized rotors. Meanwhile, the optimized rotor exhibits a higher tip vortex intensity than the original rotor. This enhancement is mainly attributed to the greater pressure difference between the pressure and suction surfaces of the blades, induced by the geometric modifications of the optimized rotor.

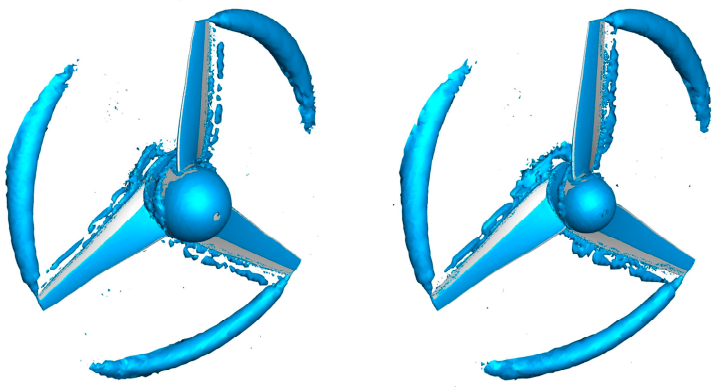

(**a**) *TSR* = 4

Figure 15. *Cont.*

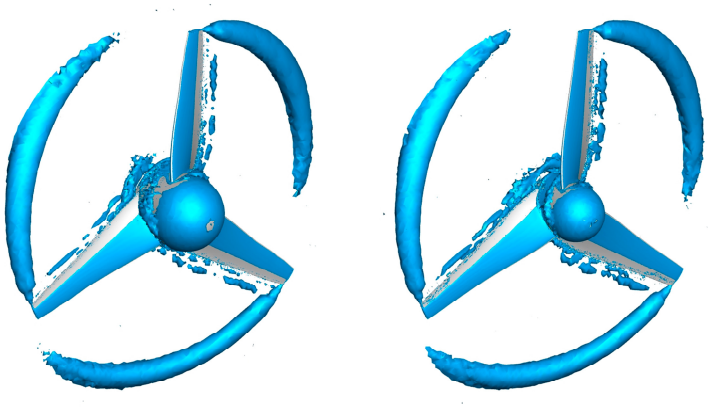

(**b**) *TSR* = 5

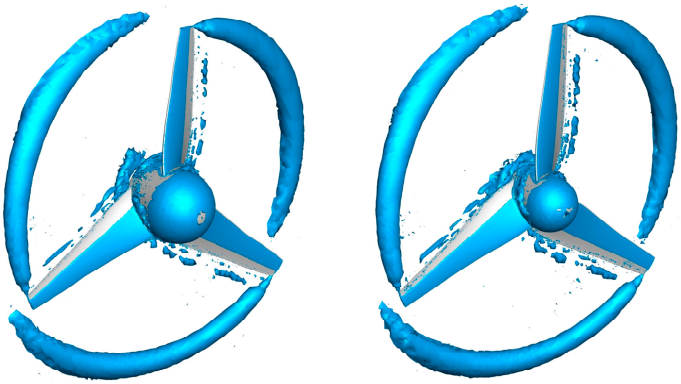

(**c**) *TSR* = 6

Figure 15. Iso-surfaces of *Q* criterion (Q = 100 s^{-2}) around the original and optimized rotor at *TSR* of 4 to 6 (**left**: original rotor; **right**: optimized rotor).

5. Conclusions

This study aims to establish a computationally efficient optimization model for a horizontal-axis wind turbine. A horizontal-axis tidal current turbine rotor was modeled in this study based on an improved BEM method. To improve the energy capture performance of the tidal energy turbine rotor, three rotor structural parameters, namely the rotor hub diameter (factor A), airfoil type (factor B), and airfoil maximum thickness (factor C), are selected as experimental factors according to the orthogonal design scheme. A 3-factor, 3-level test method is adopted, and the optimized rotor is obtained by numerical simulation. Using CFD fluid dynamics calculation software, the performance of the optimized rotor was compared in detail with that of the original rotor. The main conclusions are as follows:

1. A refined baseline rotor geometry was successfully established using an improved BEM approach incorporating tip and hub loss corrections. The performance and load of the designed rotor were predicted using Fluent 2020R1 software. The results showed that the designed rotor has good hydrodynamic performance.
2. According to the orthogonal test range analysis, the influence of each factor level on the rotor power coefficient is sorted by B > C > A. The optimal combination of parameter levels is determined to be A2, B2, and C1.
3. The power coefficient of the optimized rotor is higher than that of the original rotor under different working conditions. Under the design working condition (λ = 4), the power coefficient of the optimized rotor is 0.445, which is 3.08% higher than that of the original rotor, so the energy capture performance of the optimized rotor is better.

4. The optimized airfoil section has a larger high-pressure range on the pressure surface, which helps to optimize the load distribution on the blades and thus enhance the operational stability of the tidal energy turbine. However, the increased surface pressure difference, particularly near the blade tips, also intensifies the shed tip vortices, which may affect the life of the turbine.

In general, this paper establishes a computationally economical optimization design model for horizontal-axis tidal turbines, which provides universal technical support for turbine shape optimization in engineering applications. Nevertheless, this research relies on numerical simulations as the experimental rig is under construction, and the analysis is restricted to the design flow velocity. Detailed evaluations of structural strength and fatigue behavior were not incorporated. These aspects will be discussed in future work to further improve the reliability and applicability of the optimal tidal turbine.

Author Contributions: Conceptualization, X.Z. and Y.L.; Methodology, X.Z., Y.L. and H.F.; Resources, C.W.; Data curation, C.W. and W.W.; Validation, C.W. and W.W.; Writing–original draft, X.Z.; Writing–review & editing, H.F. All authors have read and agreed to the published version of the manuscript.

Funding: This research received no external funding.

Data Availability Statement: The original contributions presented in this study are included in the article. Further inquiries can be directed to the corresponding author.

Conflicts of Interest: Author Yan Liu, Cui Wang and Wankun Wang were employed by the company China Datang Technology Innovation Co., Ltd. The remaining authors declare that the research was conducted in the absence of any commercial or financial relationships that could be construed as a potential conflict of interest.

References

1. Li, G.; Chen, Q.; Liu, Y.; Zhu, S.; Yu, Q. Study on hydrodynamic configuration parameters of vertical-axis tidal turbine. *Pol. Marit. Res.* **2020**, *1*, 116–125. [CrossRef]
2. Bahaj, A.S.; Batten, W.M.J.; McCann, G. Experimental verifications of numerical predictions for the Hydrodynamic performance of horizontal axis marine current turbines. *Renew. Energy* **2007**, *32*, 2479–2490. [CrossRef]
3. Goundar, J.N.; Ahmed, M.R. Design of a horizontal axis tidal current turbine. *Appl. Energy* **2013**, *111*, 161–174. [CrossRef]
4. Sheng, Q.; Zhao, D.; Zhang, L. A design and numerical simulation of horizontal tidal turbine. *J. Harbin Eng. Univ.* **2014**, *35*, 389–394.
5. Chen, J.H.; Wang, X.C.; Li, H.; Jiang, C.H.; Bao, L.J. Design of the Blade under Low Flow Velocity for Horizontal Axis Tidal Current Turbine. *J. Mar. Sci. Eng.* **2020**, *8*, 989. [CrossRef]
6. Li, Z.Q.; Li, G.N.; Du, L.; Guo, H.P.; Yuan, W.X. Optimal design of horizontal axis tidal current turbine blade. *Ocean Eng.* **2023**, *271*, 113666. [CrossRef]
7. Li, C.; Liang, B.; Yuan, P.; Liu, B.; Zhao, M.; Zhang, Q.; Tan, J.; Liu, J. Tidal turbine blade design optimization based on coupled deep learning and blade element momentum theory. *Phys. Fluids* **2024**, *36*, 055110. [CrossRef]
8. Wang, Y.; Li, N. Optimization and research of tidal turbine blades based on genetic algorithm. *J. Mech. Strength* **2021**, *43*, 327–332.
9. Li, Y.; Zhang, P.; Zhang, Z. Design and optimization of pump turbine rotor based on axial flow pump transformation. *Water Resour. Power* **2024**, *42*, 152–156.
10. Wang, C. Study on the Optimal Design of Ultra-Low Specific Speed Francis Turbine. Master's Thesis, Xihua University, Chengdu, China, 2020.
11. Wang, S.M.; Zhao, F.; Tian, K. Horizontal wave flow turbine blade optimization analysis based on the theory of orthogonal design. *Ocean Eng.* **2016**, *34*, 109–116.
12. Chang, Y.H.; Chen, J.; Bao, M. Numerical Simulation of the Asymmetric Hydrofoil for Vertical Axis Tidal Turbines based on the Design of Orthogonal Experiment. *J. Eng. Therm. Energy Power* **2020**, *35*, 61–68.
13. Dai, Z.; Tan, L.; Han, B.; Han, S. Multi-Parameter Optimization Design of Axial-Flow Pump Based on Orthogonal Method. *Energies* **2022**, *15*, 9379. [CrossRef]
14. Zhang, X.; Dai, Z.; Yang, D.; Fan, H. Investigation on Optimization Design of High-Thrust-Efficiency Pump Jet Based on Orthogonal Method. *Energies* **2024**, *17*, 3551. [CrossRef]

15. Yan, Y. Research on Adaptive Yaw Technology for Horizontal Axis Tidal Energy Turbines. Master's Thesis, Northeast Normal University, Changchun, China, 2023.
16. Zhang, K.; Yang, S.; Gao, Z. The Blade Design of a Bionic Shark Fin Airfoil for a Horizontal Axis Tidal Current Turbine. *J. Energy Eng.* **2021**, *147*, 04021054. [CrossRef]
17. Song, K.; Wang, W.; Yan, Y. Numerical and experimental analysis of a diffuser-augmented micro-hydro turbine. *Ocean Eng.* **2019**, *171*, 590–602. [CrossRef]
18. Menter, F.R. Two-equation eddy-viscosity turbulence models for engineering applications. *AIAA J.* **1994**, *32*, 1598–1605. [CrossRef]
19. Yu, X.L.; Wang, S.; Yuan, P.; Tan, J.; Si, X. The study on the applicability of two turbulence models in the tidal turbine. *Period. Ocean Univ. China* **2019**, *49*, 114–120.
20. Alipour, R.; Alipour, R.; Rahimian Koloor, S.S.; Petrů, M.; Ghazanfari, S.A. On the performance of small-scale horizontal axis tidal current turbines. Part 1: One single turbine. *Sustainability* **2020**, *12*, 5985. [CrossRef]
21. Xu, B.; Shen, X.; Chen, Z.J. Blade optimization for hydrodynamic performance improvement of a horizontal axis tidal current turbine. *Ocean Eng.* **2023**, *290*, 116366. [CrossRef]
22. Wang, X.H.; Zhang, L.; Zhang, L. A simplified design method of horizontal axis tidal energy turbine blade. *Appl. Mech. Mater.* **2014**, *525*, 240–246. [CrossRef]
23. Guo, F.L.Y. Numerical investigation on the hydrodynamic characteristics of a marine propeller operating in oblique inflow. *Appl. Ocean Res.* **2019**, *93*, 101969. [CrossRef]
24. Jackson, R.S.; Amano, R.S. Experimental Study and Simulation of a Small-Scale Horizontal-Axis Wind Turbine. *J. Energy Resour. Technol.-Trans. Asme* **2017**, *139*, 051207. [CrossRef]
25. Yang, Y.; Guo, Z.; Zhang, Y.; Jinyama, H.; Li, Q. Numerical investigation of the tip vortex of a straight-bladed vertical axis wind turbine with double-blades. *Energies* **2017**, *10*, 1721. [CrossRef]